Structural and magnetic ground-state properties of γ-FeMn alloys from *ab initio* calculations

M. Ekholm[1,2,*] and I. A. Abrikosov[2]

[1]*Swedish e-Science Research Centre (SeRC), Linköping University, S-58183 Linköping, Sweden*

[2]*Department of Physics, Chemistry and Biology (IFM), Linköping University, S-58183 Linköping, Sweden*

(Received 25 May 2011; revised manuscript received 11 August 2011; published 15 September 2011)

The magnetic properties of fcc-FeMn alloys, especially at the $Fe_{0.5}Mn_{0.5}$ composition, have been the subject of intense experimental and theoretical investigations for several decades. We carry out an *ab initio* theoretical study of this system, including simultaneous optimization of structural and magnetic properties, and find that the ground state is the locally relaxed noncollinear $3Q$ antiferromagnetic structure. We also show that the two most frequently used parameterizations of the generalized gradient approximation not only fail to reproduce the equilibrium lattice constant of FeMn alloys, and consequently the magnetic properties, but also internally yield qualitatively different results. For practical studies of these alloys, which currently attract great attention, we propose a set of approximations, which is internally consistent, and brings the equilibrium lattice constant and magnetic properties in good agreement with the experiment in the whole range of alloy compositions.

DOI: 10.1103/PhysRevB.84.104423 PACS number(s): 75.50.Bb, 75.50.Ee, 71.15.Mb

I. INTRODUCTION

FeMn alloys are truly versatile materials in modern technological applications. Recent advancements in steel research rely on FeMn alloys with up to 30% Mn for greatly improved strength and ductility due to twinning- and transition-induced plasticity (TWIP and TRIP) effects.[1,2] In the spin valves of contemporary computer disk read heads and memories, stoichiometric fcc-$Fe_{0.5}Mn_{0.5}$ alloys are standard materials for pinning ferromagnetic layers due to their antiferromagnetic (AFM) properties.[3,4] To optimize the performance of such FeMn-based materials, an understanding of their microscopic properties and realistic computational models are key factors. For example, the effectiveness of the exchange bias field[5] utilized in spin valve structures depends on the type of AFM ordering,[6,7] and the performance of TWIP and TRIP steels may be related to the stacking-fault energy of the fcc phase.[2]

Kouvel and Kasper investigated the magnetic state of chemically disordered bulk fcc-$Fe_{0.75}Mn_{0.25}$ by means of neutron diffraction measurements and found long-range AFM order,[8] but the precise nature of the AFM state could not be unambiguously established. Three kinds of AFM states compatible with the measurements have been proposed: the collinear $1Q$ magnetic state, and the noncollinear $2Q$ and $3Q$ states,[8–11] which are illustrated in Fig. 1.

Endoh and Ishikawa constructed a magnetic phase diagram with approximate composition boundaries containing three magnetically homogeneous phases.[10] In the limits of low (below 20%) or high (above 65%) Mn concentration, the $1Q$ state was found. Between these points, the data were interpreted in favor of the noncollinear $3Q$ magnetic state. In contrast, Bisanti *et al*. concluded from neutron diffraction and spin-wave measurements in $Fe_{0.66}Mn_{0.34}$ that the alloy has a $1Q$ magnetic state.[12] Kennedy and Hicks performed a Mössbauer spectroscopy study of $Fe_{0.5}Mn_{0.5}$ which was claimed to rule out $1Q$, and although measurements could not distinguish between $2Q$ and $3Q$, the 3Q configuration was favored as the magnetic ground state.[13] In a study on $Fe_{0.54}Mn_{0.46}$ at very low temperatures, Kawarazaki *et al*. claimed to have found definite evidence of $3Q$ as the ground state by measuring the anisotropy of γ-ray emission.[14]

Due to the lack of experimental consensus, it is desirable to obtain an *ab initio* description of the system that is independent of empirical parameters. Being an itinerant antiferromagnetic system,[11] the FeMn alloy still represents a true challenge in electronic structure theory. Substantial efforts using *ab initio* computational methods based on density functional theory (DFT) have been devoted to finding the magnetic ground state. However, theoretical results have also turned out to be varying with the employed methods and approximations.

Kübler *et al*. considered $L1_0$-ordered $Fe_{0.5}Mn_{0.5}$ compounds using the local spin density approximation (LSDA) to the DFT exchange-correlation functional, and the atomic sphere approximation (ASA) to the potential and magnetization density. It was found that the $2Q$ magnetic state is the more favorable structure.[15] This conclusion was supported in subsequent work by different authors.[16,17] Nakamura *et al*. went beyond the ASA to include noncollinearity within the spheres, and found this contribution to stabilize the $3Q$ state.[18] Spišák and Hafner performed a study where the magnetic moments were not constrained to the symmetrical configurations in Fig. 1, but were relaxed to a self-consistent ground state.[19] A new state was then found, consisting of parallel Fe moments with the Mn moments tilted 68° away, making the net Mn magnetization opposite to that of Fe.

Using the coherent potential approximation (CPA) to consider the chemically disordered $Fe_{0.5}Mn_{0.5}$ alloy, Johnson *et al*. found that the $1Q$-ordered state is more stable than a magnetically disordered state.[20] Later CPA studies, including also the noncollinear $2Q$ and $3Q$ states, found $3Q$ to be the most favorable magnetic configuration.[17,21] However, in Ref. 17, the chemically ordered compound with $2Q$ magnetic order was, in fact, found to be more stable than the chemically disordered alloy having the $3Q$ magnetic configuration. In a supercell calculation, again relaxing the magnetic moments self-consistently, Spišák and Hafner found the ground state of chemically disordered FeMn to be an almost perfect $1Q$ magnetic state.[19] Stocks *et al*. performed first-principles spin dynamics calculations for disordered supercells to recover the $3Q$ state as more stable than $1Q$, and also demonstrated the tendency of the magnetic moments to relax locally from

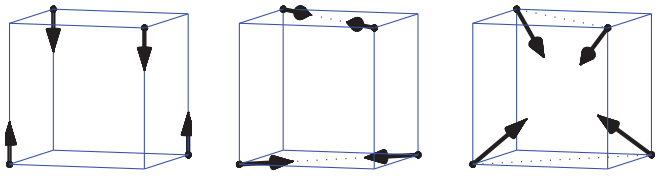

FIG. 1. (Color online) The three AFM orderings suggested as the magnetic ground state for fcc-FeMn alloys: $1Q$ (left), $2Q$, (middle), and $3Q$ (right).

the ideal $3Q$ state.[22] Common to all theoretical results is that relative energy differences between the studied magnetic states are very small, in the order of meV per atom, and as revealed by the diverse conclusions, small differences in the computational approximations can qualitatively change the results.

The purpose of the present work is twofold. First, we proceed to more accurate methods in the search for the magnetic ground state of disordered fcc-$Fe_{0.5}Mn_{0.5}$ by also taking into account local lattice relaxations as well as local magnetic reorientations. In addition, as the vast majority of the previous theoretical work for the disordered FeMn system cited above is based on the use of the LSDA for the exchange-correlation functional, in combination with the room-temperature lattice constant, we also investigate the influence of the unit cell volume, and the choice of the exchange-correlation functional parametrization, on the resulting magnetic properties of FeMn alloys. This is an interesting issue for the FeMn system since it is well known that for pure Fe, the magnetic ground state properties are very sensitive to the unit cell volume.[23] In the bcc-based α phase of Fe, the LSDA severely underestimates the equilibrium volume as compared to experiment, and thus fails to reproduce the ferromagnetic ground state. However, if the unit cell is fixed to the experimental volume, correct results are recovered. Using the generalized gradient approximation (GGA) results in an improved description of the equilibrium volume and thus correct magnetic properties.

The fcc-based γ phases of Fe and Mn are both thermodynamically stable far above room temperature.[24] γ-Fe is found in the range of 1185–1667 K (Ref. 24), but has been stabilized down to very low temperature (a few K) by precipitation in a Cu matrix,[25,26] alloying,[27] or thin film growth on a metal substrate.[28] Below the Néel temperature of $\sim$ 70 K (Refs. 29 and 30), it has been found in both experimental[31] and theoretical[32–34] studies that the magnetic ground state is strongly dependent on the lattice parameters, which, in turn, depend on the growth conditions. As a result, both an AFM state and a spin-spiral state have been reported.[35,36]

γ-Mn is stable between 1352 and 1416 K (Ref. 24), but was stabilized by Endoh and Ishikawa down to room temperature by the addition of copper or carbon.[10] In this regime, which is below the Néel temperature of 540 K, the magnetic state was concluded to be $1Q$ AFM. The local magnetic moment has been extrapolated from room-temperature measurements on FeMn alloys to be between 1.7 and 2.4 μ_B (Ref. 23). However, for fcc-Mn, LSDA has again been found to underestimate the lattice spacing, and failing to reproduce a nonzero magnetic moment. In this case, the underestimated lattice spacing is not corrected by the GGA.[37] However, calculations employing dynamical mean field theory (DMFT) in combination with the LSDA, which describes the role of Coulomb correlations beyond a local or semi-local level, have reproduced the experimental lattice spacing[37] and electronic spectrum.[38] The success of such studies, which incorporate strong many-body effects, underline the importance of $3d$-electron correlations in this system.

Unfortunately, treating strong many-body effects in alloys would be tremendously expensive from a computational point of view. The second purpose of this work is therefore to suggest a computational scheme that is internally consistent to meet the demand of an efficient yet nonempirical computational tool for practical simulations of FeMn-based materials.

This article is organized as follows: In Secs. III A and III B we consider the magnetic ground state of fcc-$Fe_{0.5}Mn_{0.5}$. In Sec. III C we include Fe- and Mn-rich alloys, and in Sec. III D we introduce the proposed computational scheme.

II. COMPUTATIONAL DETAILS

We have employed two complementary methods: the projector augmented waves (PAW)[39,40] technique, implemented in the Vienna *ab Initio* simulation package (VASP),[41–43] and the exact muffin-tin orbitals (EMTO) method[44,45] in conjunction with the full charge density technique (FCD).[46] In both methods we rely on the atomic moment approximation[23] for the description of nonuniformly magnetized systems.

In PAW calculations, chemically disordered fcc-$Fe_{0.5}Mn_{0.5}$ was modeled using a 64-atom supercell which was constructed according to the special quasirandom structure (SQS) technique,[47] as described in Ref. 48. When considering $1Q$ antiferromagnetic ordering, the magnetic moments were constrained to be either parallel or antiparallell to the global quantization axis, allowing only longitudinal relaxations. This is in contrast to the case of $2Q$ and $3Q$ orderings, where magnetic moments were allowed to relax locally from the $\langle 110\rangle$ and $\langle 111\rangle$ directions, respectively. We refer to the locally relaxed noncollinear states as $2Q_R$ and $3Q_R$. In evaluation of total energy, we employed the tetrahedron method with Blöchl corrections.[49] When relaxing ion positions, the first-order Methfessel-Paxton method[50] was used with the smearing width parameter σ set to 0.2 eV. We kept the basis set cutoff fixed to 300 eV and used a $5\times5\times5$ **k**-points mesh, from which special **k** points were chosen according to the Monkhorst-Pack scheme.[51] We have used several different approximations to the exchange-correlation functional, including the LSDA and the GGA as parametrized by Perdew-Wang (PW91)[52] and Perdew-Burke-Enzerhof (PBE).[53] When employing the PW91 functional we used the recommended Vosko-Wilkes-Nusair[54] interpolation of the Ceperly-Alder correlation energy density.[55]

We have used a scalar-relativistic implementation of the EMTO method which allows us to consider magnetic moments with arbitrary orientation. This implementation makes use of the generalized Bloch theorem[56] to constrain the magnetic moments of each atomic sphere to have a certain direction with respect to the global quantisation axis. Self-consistent relaxation of magnetic moments is then limited to their magnitudes. We used a basis set of s,p,d, and f exact

muffin-tin orbitals and converged absolute total energy to the order of 0.1 meV/atom with respect to the number of **k** points. To model chemical disorder, we have used CPA.[57,58] In the EMTO calculations, we have used the LSDA and PBE-GGA exchange-correlation functionals.

III. RESULTS

A. Fixed volume calculations fcc-$Fe_{0.5}Mn_{0.5}$

Assuming different global AFM configurations, we have calculated total energies of chemically random fcc-$Fe_{0.5}Mn_{0.5}$ with different levels of approximation to identify the roles of magnetic and ionic relaxations. We begin by keeping the unit cell volume fixed to the experimental value and use the LSDA exchange-correlation functional, which is a combination of approximations used in previous theoretical work on this system and was advocated in Ref. 59 for an accurate description of electronic structure in transition metals. In line with the literature, we have used the value 3.60 Å for the $T = 0$ K lattice constant, which was obtained in Ref. 15 by extrapolation from experimental data, and corresponds to the unit cell volume of 11.7 Å^3. At room temperature, the lattice constant has been reported to be 3.63 Å (Refs. 10 and 60), corresponding to the unit cell volume 12.0 Å^3.

Using the EMTO-CPA method to consider the ideal fcc crystal lattice we have calculated total energy as a function of the tilt angle θ, which determines the type of AFM ordering as illustrated in Fig. 2. As θ is increased, the magnetic configuration goes continuously from the $1Q$ state at $\theta = 0$ through the $3Q$ state at $\theta = 0.3\pi$ and $2Q$ at $\theta = 0.5\pi$. Figures 3 and 4 show the results obtained at zero- and room-temperature lattice constants, respectively. We find that the total energy is minimized by the $3Q$ configuration, followed by $2Q$ and $1Q$. Since

$$E(\theta \pm \pi) = E(\theta), \tag{1}$$

by symmetry, these calculations for the ideal fcc lattice suggest that the $3Q$ state constitutes the only energy minimum, while $2Q$ and $1Q$ seem to be unstable against variations in θ.

Using the PAW method on the ideal fcc lattice we include relaxation of magnetic moments from the ideal ⟨111⟩ and ⟨110⟩ directions in noncollinear supercell calculations. As

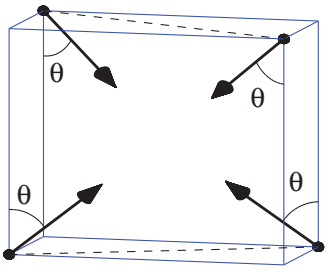

FIG. 2. (Color online) Illustration of the tilt angle θ, determining the type of AFM state. $\theta = 0$ corresponds to $1Q$ configuration. As θ is increased, the moments of the magnetic unit cell are tilted toward a common center, resulting in $3Q$ at $\theta = \arccos(\frac{1}{\sqrt{3}}) \approx 0.30\pi$ and $2Q$ at $\theta = \pi/2$. Dashed lines connect the bases of magnetic moments that are tilted within a common plane.

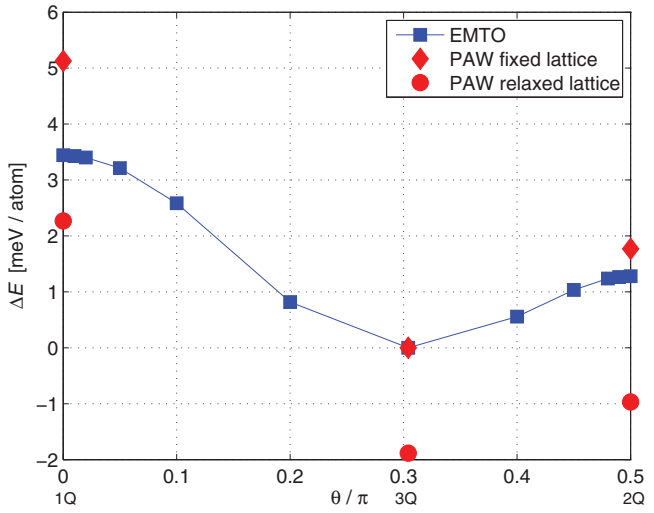

(a)Total energy

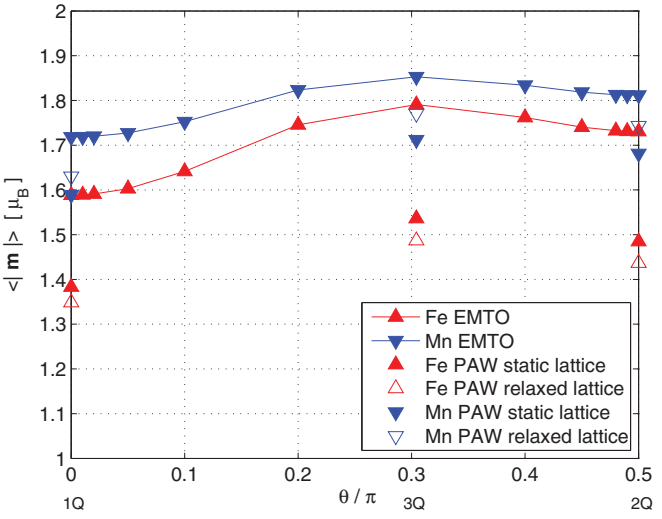

(b)Average magnetic moments

FIG. 3. (Color online) (a) Total energy and (b) average magnetic moments as a function of the tilt angle θ in chemically disordered fcc-$Fe_{0.5}Mn_{0.5}$ at the experimental lattice constant $a = 3.60$ Å obtained with the EMTO-CPA (squares) and PAW supercell methods for ideal (diamonds) and locally relaxed (circles) lattices using the LSDA functional.

seen in Figs. 3 and 4, these results do not influence the conclusions derived from EMTO-CPA calculations concerning the $1Q$–$2Q$–$3Q$ relationships. Comparing Figs. 3 and 4 we also note that thermal expansion increases the $1Q$–$3Q$ energy difference. The results presented so far are in agreement with Refs. 17, 21, and 22 although the $1Q$–$3Q$ energy difference is larger in Refs. 21 and 22. However, it should be noted that the energy scale is very small, and differences in computational methodology may be responsible for quantitative differences between earlier results and ours.

As mentioned in Sec. II, to distinguish the magnetic states with local moments deviating from the ideal $2Q$ and $3Q$ orientations, we refer to them as $2Q_R$ and $3Q_R$. We have calculated the magnitude of the local reorientations by

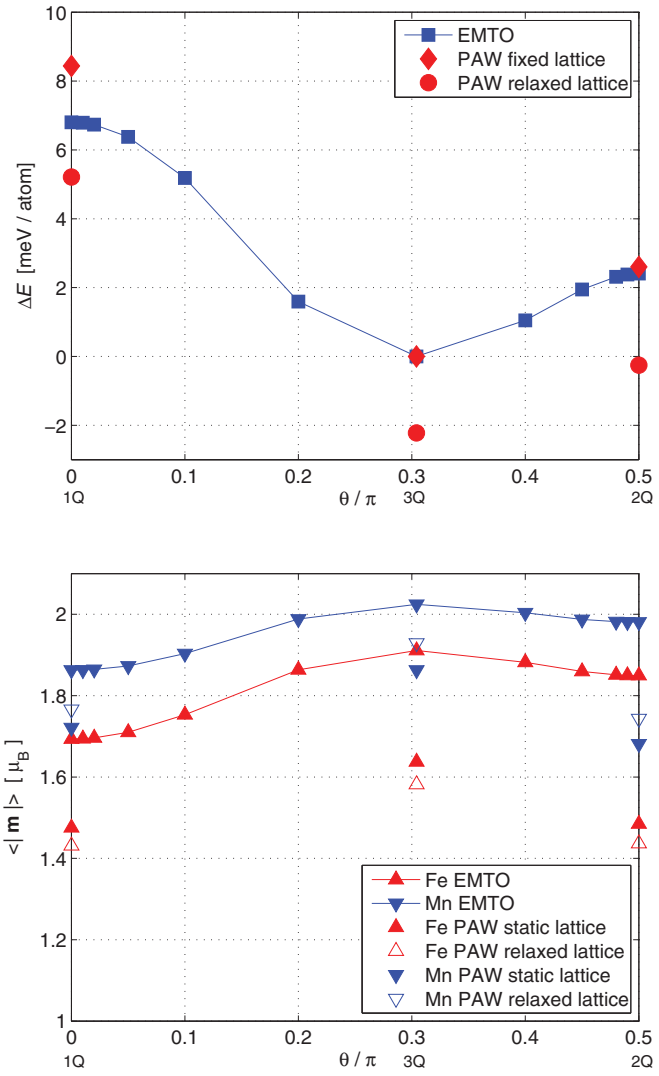

FIG. 4. (Color online) Same quantities as in Fig. 3 but calculated at the room-temperature lattice constant of 3.63 Å.

computing the average angle between the ideal and relaxed orientations of the moments:

$$\langle \alpha \rangle = \frac{1}{N} \sum_{i=1}^{N} \arccos \frac{\mathbf{m}_i \cdot \mathbf{m}_i^{\mathrm{R}}}{|\mathbf{m}_i| |\mathbf{m}_i^{\mathrm{R}}|}, \qquad (2)$$

taken over the $N = 64$ atoms of the supercell. For the $3Q_{\mathrm{R}}$ state, the average deviation is 9° for both Fe and Mn moments at zero temperature, as well as for the room-temperature volume; this is in agreement with the results obtained in the spin dynamics calculations by Stocks *et al.*[22] The magnitudes of the magnetic moments obtained with the CPA and supercell methods are in good agreement, as seen in Fig. 3(b). Average Fe and Mn magnetic moments are close in magnitude and take their largest values in the $3Q$ magnetic state. Previous theoretical work for disordered fcc-$Fe_{0.5}Mn_{0.5}$ using the present set of approximations have reported Fe moments in the range of 1.48–1.79 μ_{B} and Mn in the range of 1.58–2.17 μ_{B}, which typically is the largest.[17,19,21,22] In the experiment of Endoh and Ishikawa, the moments were reported to be significantly lower, only 1 μ_{B} for both Fe and Mn atoms at the stoichiometric composition.

Including also local relaxations of the ions from the ideal fcc lattice sites has the effect of lowering the total energy by an amount approximately equal to the $1Q$–$3Q_{\mathrm{R}}$ energy difference itself. However, the shift is rather independent of magnetic configuration, and for $3Q_{\mathrm{R}}$ the ion drift is, on average, 0.02 Å, and 0.03 Å, for Fe and Mn, respectively. The average angle of reorientation for $3Q_{\mathrm{R}}$ is again found to be approximately 9° at both lattice constants. As seen in Fig. 3(b), the magnetic moments are shifted to lower values with the inclusion of local lattice relaxations, bringing them in closer agreement with experiment. Nevertheless, the internal relations between the $1Q$, $2Q$, and $3Q$ configurations are well captured even in the absence of local environment effects, and CPA-based methods may be used with confidence for practical purposes.

Based on the above results we conclude $3Q_{\mathrm{R}}$ to be the magnetic ground state of fcc-$Fe_{0.5}Mn_{0.5}$, in line with the results in Ref. 22 for chemically disordered FeMn. We will next investigate the ground state magnetic configuration including unit cell optimization.

B. Unit cell optimization for γ-$Fe_{0.5}Mn_{0.5}$

1. *Lattice constant of cubic structure*

Using the LSDA functional, we find from EMTO-CPA calculations the equilibrium unit cell volume of 10.0 Å^3 for fcc-$Fe_{0.5}Mn_{0.5}$. The equilibrium volume, which corresponds to the lattice constant of 3.42 Å, is thus severely underestimated compared to the experimental value of 11.7 Å^3. This failure of LSDA is not unexpected since it is known to overbind both Fe and Mn, as discussed in Sec. I.

Total energy for the $1Q$, $2Q$, and $3Q$ magnetic configurations are very close around the equilibrium, but the $1Q$ magnetic state is lower than the $2Q$ and $3Q$ states by 0.5 and 0.8 meV, respectively. At ∼11.3 Å^3, we find the total energy of the $1Q$, $2Q$, and $3Q$ configurations to be degenerate, and with increasing volume we find the $3Q$ configuration to be the more favorable state, as in the previous section.

In Fig. 5(a) we show the total energy as a function of unit cell volume and lattice constant, calculated with the PBE-GGA functional for the one-electron potential and the total energy. The equilibrium volume is 11.1 Å^3, assumed for the $1Q$ configuration, which corresponds to the lattice constant of 3.54 Å, which is 1.7% smaller than the 0 K experimental value. In other words, although the GGA improves the lattice constant, it does not correct the overbinding of the LSDA, and the magnetic configuration at equilibrium is the same as obtained with LSDA. We also see in Fig. 5(a) that, at the experimental volume, $3Q$ is again more favorable, in line with the LSDA results.

In Figs. 5(b) and 5(c) we show magnetic moments calculated with the PBE-GGA functional, which are seen to be larger as compared to the LSDA results in Fig. 3(b), and consequently in worse agreement with the experiment. This may be expected as the GGA functional overestimates magnetic energy.[59]

Using the PAW method with the PBE-GGA functional on the ideal fcc lattice to include local magnetic relaxations, we obtain results in good agreement with EMTO-CPA, favoring the $1Q$ magnetic state at the equilibrium lattice parameter

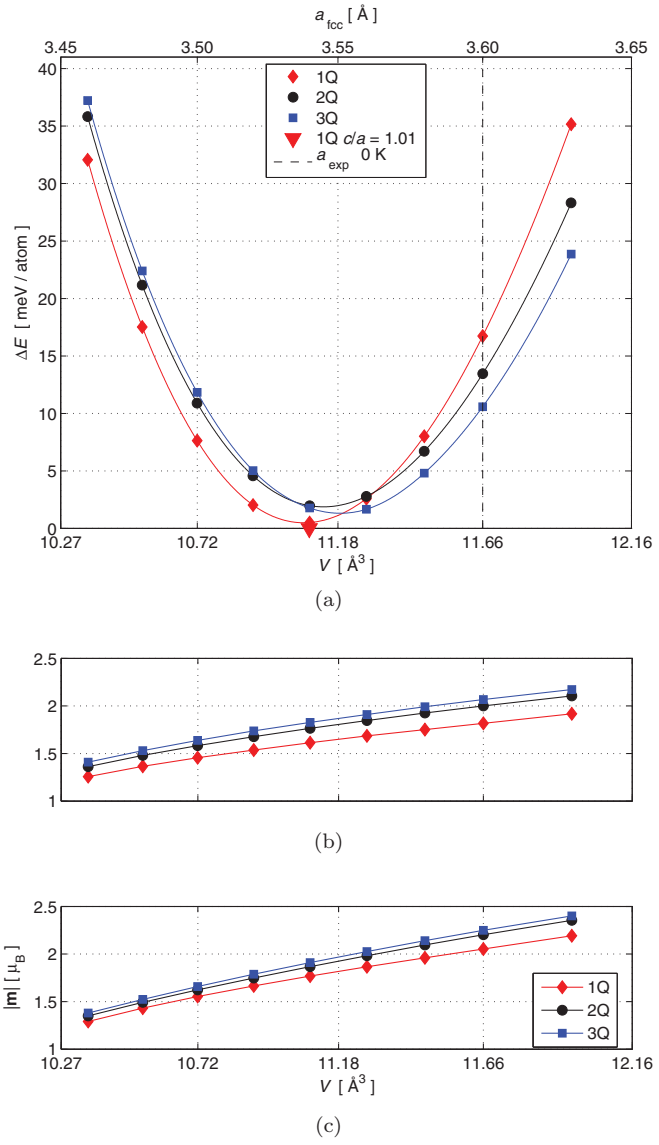

FIG. 5. (Color online) (a) Total energy and magnetic moments for (b) Fe and (c) Mn atoms in $Fe_{0.5}Mn_{0.5}$, calculated with the EMTO-CPA method and the PBE-GGA exchange-correlation functional for cubic fcc structure assuming $1Q$ (red diamonds), $2Q$ (black circles), and $3Q$ (blue squares) magnetic structure, as a function of unit cell volume (lower horizontal scale) and the lattice constant (upper horizontal scale). The red triangle shows the total energy for the tetragonally distorted fct structure assuming $1Q$ ordering at the ground state volume. In this case, it is very close to the ground state volume obtained for $1Q$ order in fcc. The experimental unit cell volume corresponding to 0 K is shown as a vertical dashed line.

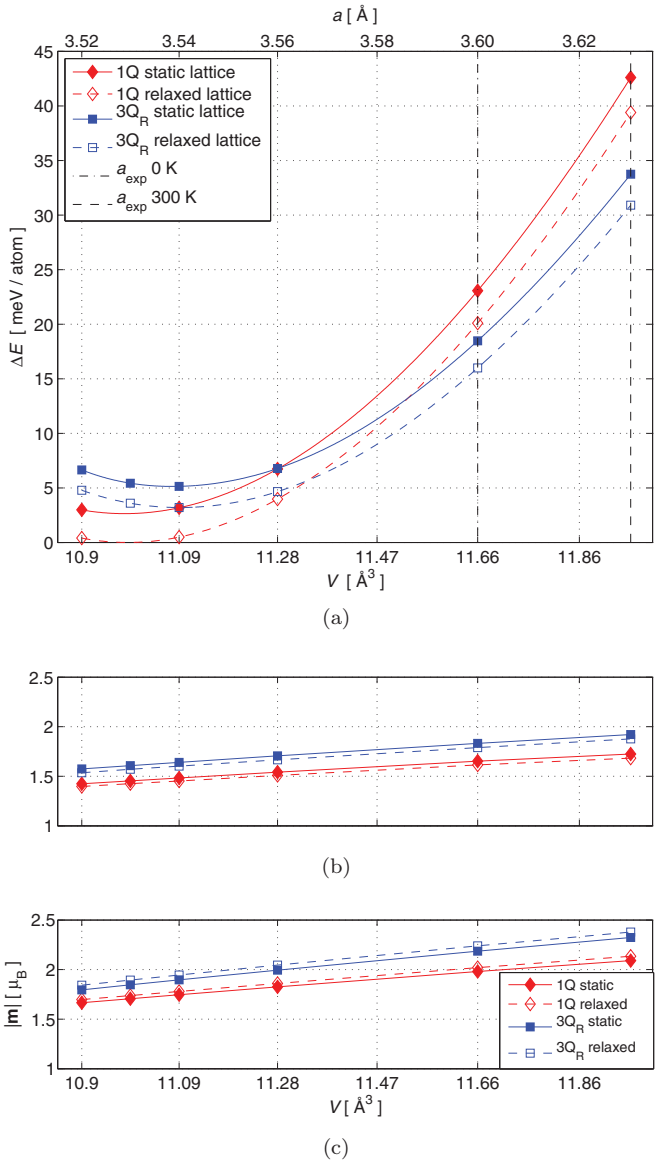

FIG. 6. (Color online) (a) Total energy and average magnetic moments for (b) Fe and (c) Mn atoms in fcc-$Fe_{0.5}Mn_{0.5}$, assuming the $1Q$ and $3Q_R$ magnetic states calculated with the PAW supercell method using the PBE-GGA exchange-correlation functional. Solid lines/filled symbols represent calculations on a static lattice and dashed lines/open symbols represent calculations including local lattice relaxations. In (a), red diamonds indicate $1Q$ state and blue squares indicate the $3Q_R$ state. The experimental unit cell volume corresponding to 0 and 300 K are shown as dash-dotted and dashed vertical lines, respectively.

3.53 Å, but holding $3Q_R$ more favorable at larger volume, as shown in Fig. 6(a). Average magnetic moments, presented in Figs. 6(b) and 6(c), are also in very good agreement with those found with the EMTO-CPA method. We also note that local lattice relaxations lower the Fe magnetic moments and increase the Mn moments, but do not change the $1Q$–$3Q_R$ energy relationship or the theoretical equilibrium lattice constant significantly.

The average angles of magnetic moment deviations from the ideal ⟨111⟩ orientations on the relaxed lattice, defined in Eq. (2), are between 9° and 10°, depending on volume. We find 80% of the magnetic moments within 16° of the ideal ⟨111⟩ orientations. These results are close to what was obtained in the preceding section using LSDA at the experimental lattice constant.

Changing the parametrization of the GGA functional from PBE to PW91, the situation concerning $1Q$–$3Q_R$ becomes slightly different. For the ideal fcc lattice we obtain $3Q_R$ as the ground state at approximately the same equilibrium lattice constant as found using the PBE parametrization,

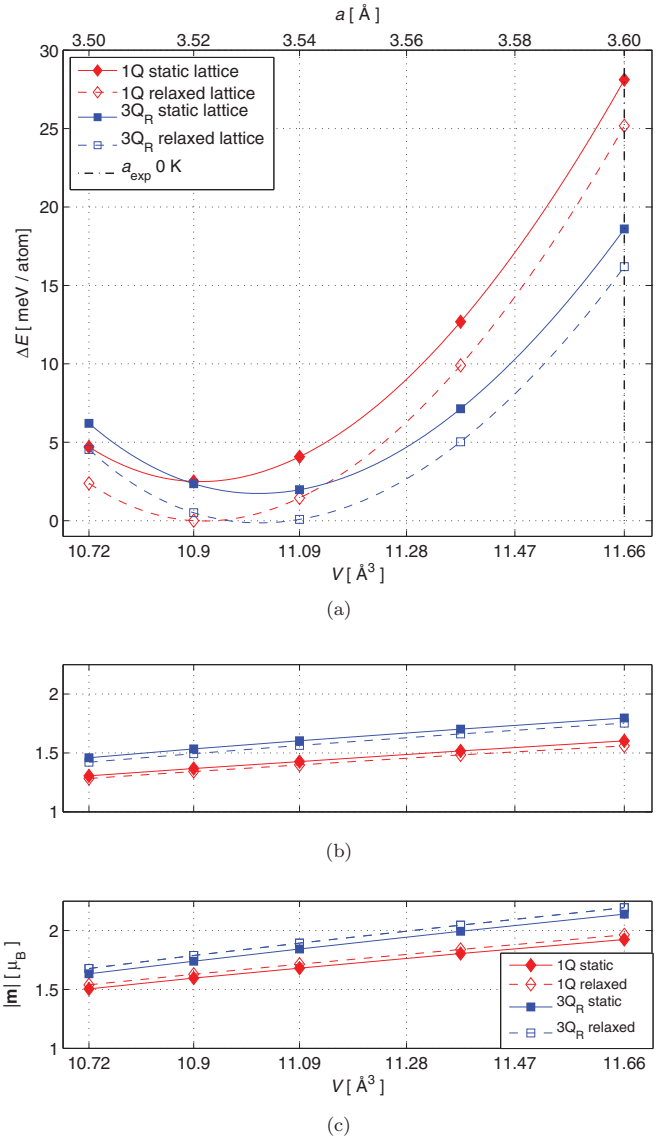

FIG. 7. (Color online) Same quantities as in Fig. 6 but calculated with the PW91 exchange-correlation functional.

as seen in Fig. 7, though with slightly smaller magnetic moments. Including local lattice relaxations results in a slight preference of $3Q_R$, but the minima are so close that they must be considered degenerate. Thus, there is a clear discrepancy between the results from the PBE- and PW91-GGA functionals, which is also observed in fcc-Fe (Ref. 61). However, we also note that at experimental volumes, $3Q_R$ solution is again obtained as the magnetic ground state, in agreement with all other computational methods considered so far.

These facts—that by using the PBE-GGA functional we obtain the $1Q$ configuration as the magnetic ground state at equilibrium volume, but using instead the PW91-GGA functional we find the $3Q$ state to be degenerate with the $1Q$ state, or even more favorable depending on if local lattice relaxations are included—point out the intricate magnetic effects of this system, which apparently are not adequately described by DFT methods based on local (LSDA) or semi-local (GGA) exchange-correlation functionals.

2. Spin spiral states

As our PBE-GGA calculations assuming the $1Q$, $2Q$, and $3Q$ states fail to reproduce the experimental lattice constant in fcc-$Fe_{0.5}Mn_{0.5}$, and indicate the $1Q$ state as the ground state magnetic configuration, we have calculated the total energy of various planar spin-spiral states, which includes the $1Q$ state.

In an experimental study of pure γ-Fe, Tsunoda *et al.* reported a state with wave vector **q** along the line connecting the X and W points of the fcc Brillouin zone.[36] Theoretical work has subsequently found several other metastable spin-spiral states along the Γ–X line, depending sensitively on volume.[32–34]

Using the EMTO method, we have restricted **q** along lines connecting certain points of interest in the Brillouin zone, and optimized the lattice constant for each value of **q** with the PBE-GGA functional. For comparison, we have also performed calculations using the LSDA functional at the experimental lattice constant corresponding to 0 K.

Figure 8 shows results for the cubic fcc-$Fe_{0.5}Mn_{0.5}$ alloy. GGA and LSDA results are in good agreement and indicate the total energy to be minimized at the X point, which corresponds to the $1Q$ magnetic configuration, with large Fe and Mn moments. We also find several metastable states, at the K and L points, as well as on the Γ–X, Γ–K, and L–Γ lines. A further inspection of Fig. 8(b), reveals that the Γ point actually corresponds to a collinear disordered ferrimagnetic state, where the randomly distributed Fe and Mn atoms have magnetic moments antiparallel to each other.

The most significant feature seen in Fig. 8(a) is, however, that the energy difference between the X point and the other spin spiral states investigated in this work is very large compared to the $1Q$–$3Q$ energy difference. We may therefore exclude these spin spiral states from further discussion of the magnetic ground state.

3. Tetragonal distortions

Due to the tetragonal symmetry of the $1Q$ AFM state, it may be associated with tetragonal distortions of the underlying lattice from cubic symmetry. In γ-Fe stabilized below the Néel temperature, the crystal structure of the $1Q$-ordered phase has indeed been found to show tetragonal distortions.[62] Theoretical calculations for pure $1Q$-Fe using LSDA at the experimental unit cell volume have yielded $(c/a)_0 = 1.08$ (Refs. 63 and 64). With the EMTO method, we obtain the unit cell volume of 10.9 Å^3 for pure fct-Fe, which is close to what has been reported in previous GGA calculations.[65] The c/a ratio is 1.09, which is in good agreement with previous work employing LSDA at the experimental lattice constant,[63,64] and with GGA at equilibrium.[65]

For pure γ-Mn at room temperature, Endoh and Ishikawa found the value $(c/a)_0 = 0.945$ and the $1Q$ AFM configuration. The local magnetic moment extrapolated to 0 K was found to be 2.1 μ_B. A theoretical explanation for the relation between the magnetic ordering and the distortion has been provided by Oguchi and Freeman,[66] and the observed contraction along the AFM planes of γ-Mn has been reproduced several times

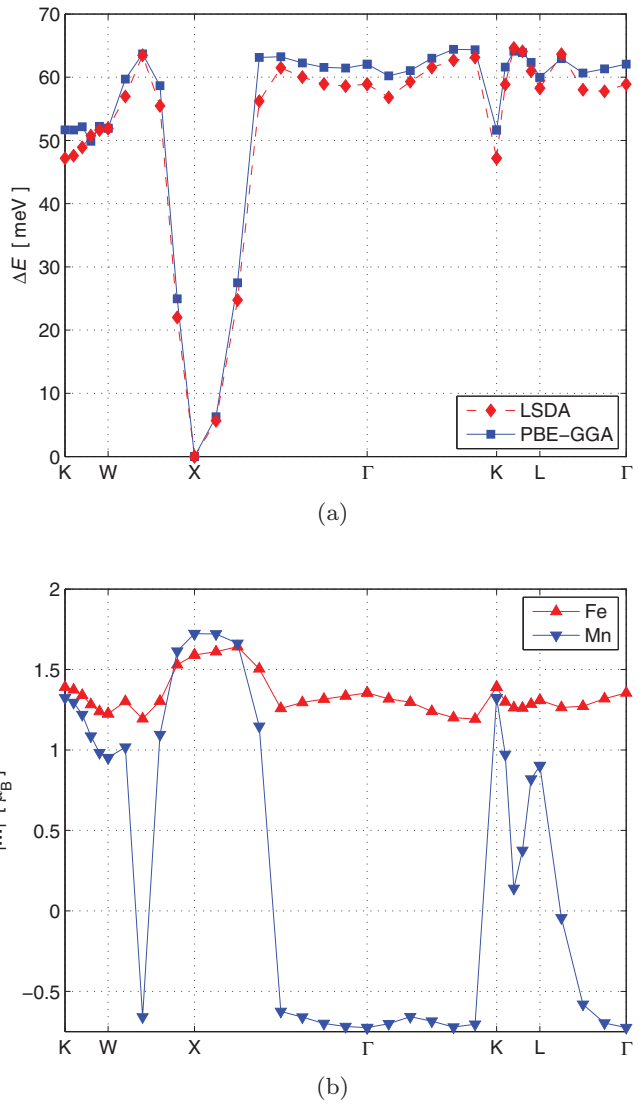

FIG. 8. (Color online) (a) Total energy and (b) magnetic moments in the $Fe_{0.5}Mn_{0.5}$ alloy calculated for planar spin spirals along lines connecting certain high symmetry points of the fcc Brillouin zone. In (a), total energy obtained using PBE-GGA exchange-correlation functional is shown by blue squares and solid line, while LSDA results are shown by red diamonds and dashed line. In (b), the magnetic moments, for Fe are given by red triangles pointing up, while Mn moments are given by blue triangles pointing down. The magnetic moments shown are calculated with the LSDA functional.

in calculations,[64,67–69] However, the experimental volume is significantly underestimated in calculations based on LSDA and GGA.[37,68,69] We obtain the unit cell volume of 11.5 Å^3 and $(c/a)_0 = 0.93$, and the magnetic moment 2.2 μ_B. These results are in reasonable agreement with previous theoretical studies employing comparable methods.[69] Theory is thus able to reproduce the experimental c/a ratio, although the unit cell volume is underestimated compared to the experimental value of 12.9 Å^3 (Ref. 10).

Since the end compounds show tetragonal contraction and expansion it is interesting to investigate if the ground state of the stoichiometric alloy deviates significantly from cubic fcc structure. We have therefore relaxed the c/a ratio and volume of $1Q$ fct-$Fe_{0.5}Mn_{0.5}$ using the EMTO-CPA method with the PBE-GGA functional. As seen in Fig. 5(a), we obtain a slight tetragonal distortion with $(c/a)_0 = 1.01$ at the unit cell volume of 11.1 Å^3. However, total energy for fct is lower than for fcc by less than 0.5 meV/atom, which is very little, and we conclude that tetragonal distortions are of lesser importance at this composition.

C. Off-stoichiometric compositions

Having performed a detailed analysis of our calculations for the γ phase of the $Fe_{0.5}Mn_{0.5}$ alloy, we will now consider the concentration dependence of the obtained results. We have chosen compositions in the two $1Q$ fields of the magnetic phase diagram of Ref. 10. Calculations were carried out using the EMTO-CPA method, which readily allows any composition to be considered.

Starting on the Fe-rich side of the phase diagram, we have calculated total energy as a function of volume for $Fe_{0.9}Mn_{0.1}$, which is displayed in Fig. 9. The results indicate that the $3Q$ configuration is the magnetic ground state, which is not in agreement with the magnetic phase diagram in Ref. 10. Comparing with the room-temperature experimental volume 11.5 Å^3, obtained from interpolation of the data in Refs. 10 and 60, we may conclude that our value of 10.8 Å^3 is also an underestimation. Due to the contracted volume, magnetic moments, shown in Figs. 9(b) and 9(c), are also clearly underestimated at the equilibrium volume, compared to the experimental average value of 2.0 μ_B, which was found by extrapolation to 0 K (Ref. 10). However, magnetic moments obtained at the experimental volume agree quite well.

Although Endoh and Ishikawa found the crystal structure to be cubic fcc at this composition (with the addition of other elements),[10] we have relaxed the c/a ratio while assuming the $1Q$ magnetic state. We find that as the cubic constraint is removed, the lattice goes through nonnegligible tetragonal distortions, ending at $(c/a)_0 = 1.08$ at the unit cell volume of 10.9 Å^3, as shown in Fig. 9. Clearly, the energy gain from tetragonal distortions is greater than the $1Q$–$3Q$ difference, and we find that $1Q$-fct is more stable than $3Q$-fcc at the theoretical equilibrium volume. This is in agreement with the experimental magnetic phase diagram, although the unit cell volume is still strongly underestimated.

On the Mn-rich side of the phase diagram, we have considered the $Fe_{0.2}Mn_{0.8}$ alloy. Calculations for the cubic fcc crystal structure, shown in Fig. 10, yield the equilibrium unit cell volume of of 11.3 Å^3, and the $1Q$ magnetic state. Although the obtained magnetic configuration agrees with Ref. 10, we again observe a large discrepancy when comparing with the reported unit cell volume, which is 12.3 Å^3. Relaxing the c/a ratio we obtain $(c/a)_0 = 0.97$ at the volume 11.3 Å^3, and although the $1Q$-fct state is lower than any cubic fcc-state we have considered at this composition, the gain in total energy is not as dramatic as on the Fe-rich side.

Table I summarizes our results for the lattice constant of cubic fcc-FeMn alloys, which are compared with experimental values. Allowing tetragonal distortions in the $1Q$ state leads to new ground states at c/a ratios in good agreement with experiment. However, it is also clear at this stage that the present parametrizations of the GGA functional do not

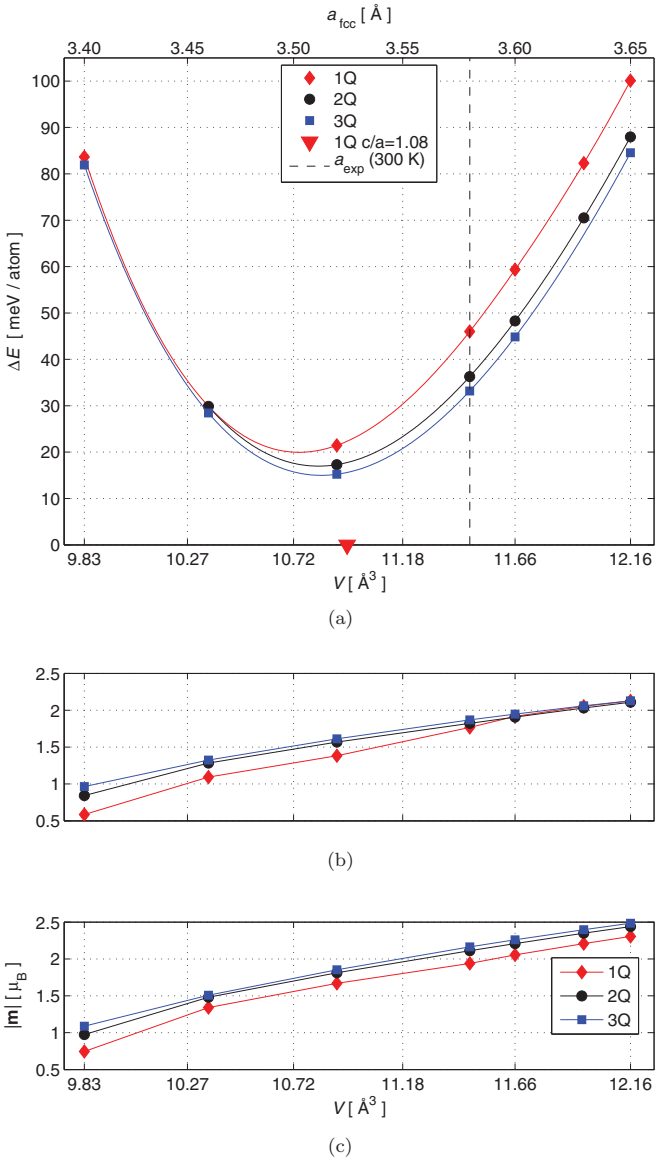

FIG. 9. (Color online) (a) Total energy and magnetic moments for (b) Fe and (c) Mn atoms in $Fe_{0.9}Mn_{0.1}$, calculated with the EMTO-CPA method and the PBE-GGA exchange-correlation functional for cubic fcc structure assuming $1Q$ (red diamonds), $2Q$ (black circles), and $3Q$ (blue squares) magnetic structure, as a function of unit cell volume (lower horizontal scale) and the lattice constant (upper horizontal scale). The red triangle shows the total energy for the tetragonally distorted fct structure assuming $1Q$ ordering at the ground state volume. The experimental unit cell volume corresponding to 300 K is shown as a vertical dashed line.

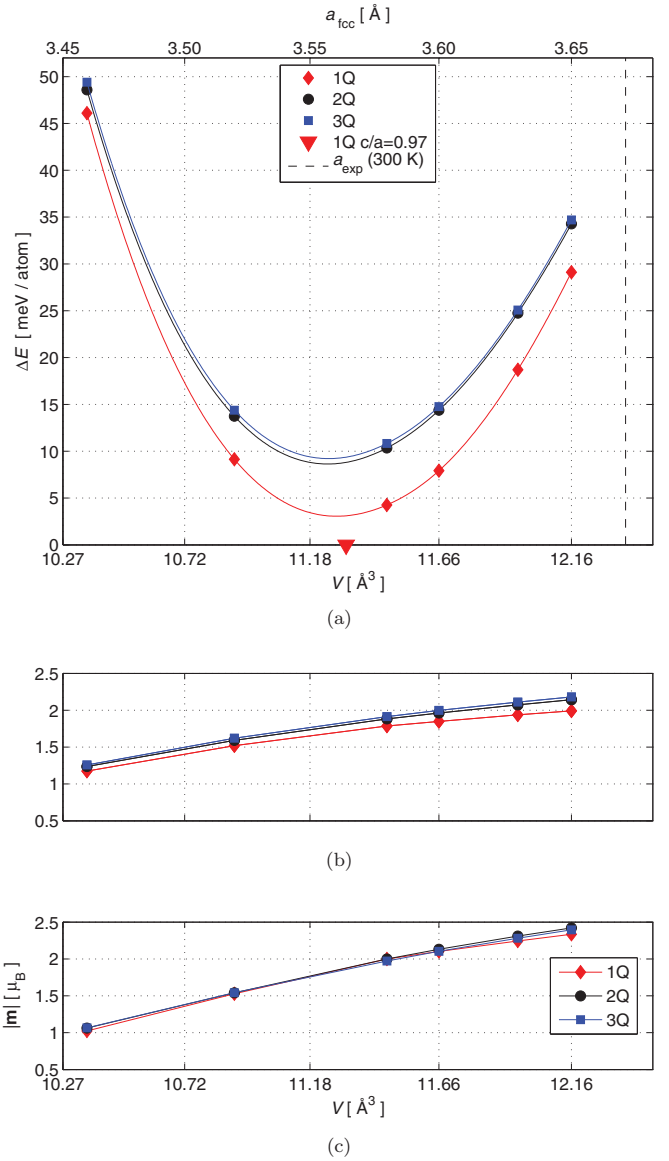

FIG. 10. (Color online) (a) Total energy and magnetic moments for (b) Fe and (c) Mn atoms in $Fe_{0.2}Mn_{0.8}$, calculated with the EMTO-CPA method and the PBE-GGA exchange-correlation functional for cubic fcc structure assuming $1Q$ (red diamonds), $2Q$ (black circles), and $3Q$ (blue squares) magnetic structure, as a function of unit cell volume (lower horizontal scale) and the lattice constant (upper horizontal scale). The red triangle shows the total energy for the tetragonally distorted fct structure assuming $1Q$ ordering at the ground state volume. The experimental unit cell volume corresponding to 300 K is shown as a vertical dashed line.

accurately reproduce experimental values for the unit cell volume of FeMn alloys, and that the disagreement worsens with the increased concentration of Mn.

D. A practical scheme for calculations of FeMn alloys

As the unit cell volumes determined in the preceding sections are consistently underestimated using both the EMTO-CPA and PAW supercell methods, employing the LSDA, PBE-GGA, and PW91-GGA functionals, we conclude that state-of-the-art local and semi-local exchange-correlation functionals may not be sufficiently accurate to describe the FeMn alloy system. However, due to the industrial importance of FeMn alloys, and the great need to find a theoretical description beyond empirical models that is internally consistent and agrees with experiment, we will demonstrate a computational scheme that is free of adjustable parameters and that reproduces experimental data, at least for the lattice parameter and magnetic properties. This scheme consists of

TABLE I. Calculated equilibrium lattice parameters for cubic fcc-$Fe_{1-x}Mn_x$ alloys, and comparisons with experimental values.

	a_0 [Å]			
x	PAW	EMTO	EMTO + frozen-core	experiment
0.8		3.56	3.65	3.67[a]
0.5	3.53	3.54	3.63	3.60[b], 3.63[c]
0.1		3.51	3.58	3.58[d]
0.0	3.50	3.50	3.56	3.58[e]

[a]300 K, Ref. 10 and extrapolation from values in Ref. 60.
[b]Extrapolation to 0 K Ref. 15.
[c]300 K, Refs. 10 and 60.
[d]300 K, extrapolation from values in Refs. 10 and 60.
[e]70 K, Refs. 62 and 76.

two choices of approximations, one concerns the description of magnetism and the other one total energy.

In Secs. III D 1 and III D 2 we will show the individual impact of each approximation on the equilibrium structural and magnetic properties, before we demonstrate in Sec. III D 3 their performance when combined in the actual scheme.

1. Using LSDA charge density in the GGA functional for total energy

As we have seen in Sec. III B 1, the total energy obtained with GGA results in a better description of equilibrium volume than that obtained by LSDA. At the same time, we have also demonstrated in Sec. III A, that the self-consistent charge density generated by the LSDA provides a better description of magnetic moments, and presumably even the magnetic ground state, if used in combination with the experimental lattice parameter.

In this section we demonstrate that it is possible to improve the variation of LSDA energy with volume by including gradient corrections, by means of using LSDA to calculate self-consistent charge density, n_0^{LSDA}, and degree of magnetization. This charge density can then be used to evaluate the exchange-correlation contribution to the total energy as

$$E_{\mathrm{xc}} = \int d^3r f\left(n_{0,\uparrow}^{\mathrm{LSDA}}, n_{0,\downarrow}^{\mathrm{LSDA}}, \nabla n_{0,\uparrow}^{\mathrm{LSDA}}, \nabla n_{0,\downarrow}^{\mathrm{LSDA}}\right). \quad (3)$$

This methodology was successfully applied to FeNi alloys in Ref. 70, where it was also explicitly demonstrated that the scheme leads to very similar values of lattice parameters as compared to fully self-consistent GGA calculations.

We have therefore recalculated equilibrium properties of FeMn alloys with the EMTO method using the LSDA functional during the Kohn-Sham iterations to find the nonspherical charge density and magnetic moments, and then evaluating total energy on that charge density, using the PBE form of the function f.

The total energy obtained in this way for the fcc-$Fe_{0.5}Mn_{0.5}$ alloy is shown in Fig. 11(a), which may be compared with the energy presented in Fig. 5(a), obtained with the standard implementation of using the same exchange-correlation potential for evaluating both charge density and total energy. Equilibrium volumes for the $1Q$, $2Q$, and $3Q$ magnetic states are essentially the same. However, total energy for the $1Q$ state

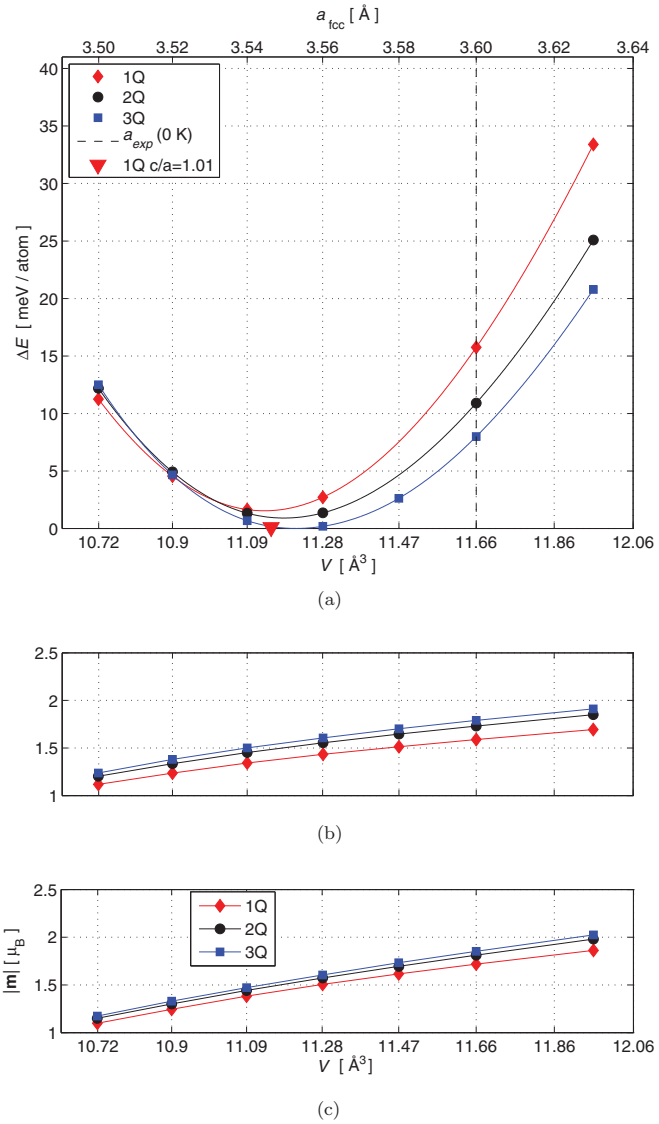

FIG. 11. (Color online) (a) Total energy and magnetic moments for (b) Fe and (c) Mn atoms in $Fe_{0.5}Mn_{0.5}$, calculated with the EMTO-CPA method, using the LSDA functional to compute the self-consistent charge density and magnetic moments, and then evaluating total energy using this charge density in the GGA functional. In (a) the total energy is shown for the cubic fcc structure assuming $1Q$ (red diamonds), $2Q$ (black circles), and $3Q$ (blue squares) magnetic structure, as a function of unit cell volume (lower horizontal scale) and the lattice constant (upper horizontal scale). The red triangle shows the total energy for the tetragonally distorted fct structure assuming $1Q$ ordering at the ground state volume. The experimental unit cell volume corresponding to 0 K is shown as a vertical dashed line.

is shifted up with respect to $2Q$ and $3Q$. This means that $3Q$ is obtained as the magnetic ground state at equilibrium volume followed by $2Q$, in agreement with LSDA results obtained at the experimental volume. The magnetic moments, which are evaluated on the LSDA spin-dependent charge density, are smaller than those shown in Figs. 5(b) and 5(c), bringing the results in better agreement with the experimental value of 1 μ_{B}.

It is also interesting to note that with this set of approximations, we obtain Fe and Mn magnetic moments closer to each other, which is in line with the measurements reported in Ref. 10. Relaxing the c/a ratio for the $1Q$ state, we obtain the same small tetragonal distortion as with fully self-consistent GGA; $(c/a)_0 = 1.01$, albeit with a small expansion in volume to 11.2 Å^3. As indicated in Fig. 11(a), this state is comparable in energy to the fcc $3Q$ state, the difference being only 0.1 meV/atom.

Using the same approximation scheme for the $Fe_{0.9}Mn_{0.1}$ alloy, we obtain the results shown in Fig. 12. Comparing equilibrium volumes and magnetic states with those presented in Fig. 9, we find these results to be in close agreement, except for a slightly increased tetragonal distortion of 1.09. The difference lies in the magnetic moments, which again are lower within this approximation. For $Fe_{0.2}Mn_{0.8}$ alloy, we again find the tetragonal $1Q$ fct state to be lower in energy than the $1Q$ state on the cubic fcc lattice, as shown in Fig. 13. Magnetic moments are again significantly lower in magnitude than those shown in Fig. 10.

Thus, for the off-stoichiometric compositions considered in Sec. III C, we obtain within this approximation the same equilibrium volumes and magnetic ground states as found in Sec. III C from unconstrained EMTO-CPA calculations. However, we observe a lower value of the magnetic moments, which is more in line with experiment than what was obtained in Secs. III B 1 and III C.

The method of using LSDA for the calculation of charge density—and hence magnetic properties—in combination with the GGA for the evaluation of total energy, may thus be used in calculations of FeMn alloys. This combination of approximations gives the same bonding properties as fully self-consistent GGA calculations, but an improved description of magnetism. It should be noted that the approximation demonstrated in this section is based on physical arguments. However, it does not solve the major shortcoming of either the LSDA or the GGA functional, namely the severely underestimated lattice parameters. In the following section we shall demonstrate the next level of approximation in our suggested scheme.

2. *EMTO-calculations within the frozen-core approximation*

We have tested the so-called frozen-core approximation for FeMn alloys in combination with the EMTO basis set. In this section we use the PBE-GGA functional for both the charge density and total energy calculations to compare with the results obtained in Sec. III B 1 for volumes and Sec. III A for magnetic properties.

Our results for $Fe_{0.5}Mn_{0.5}$ in the $1Q$, $2Q$, and $3Q$ magnetic states are shown in Fig. 14. For the cubic fcc lattice, the lattice parameter obtained within this approximation is 3.63 Å, corresponding to the unit cell volume of 12.0 Å^3. The lattice constant is less than 1% larger than the experimental value deduced for 0 K, which is a typical result of a GGA calculation, and is in better agreement with experiment than any other approximation used in this work. Equilibrium values of the lattice parameters using the EMTO method in combination with the frozen-core approximation are also summarized in Table I. The magnetic ground state at equilibrium volume is also found to be $3Q$—in agreement with LSDA and GGA calculations at the experimental volume and the majority of the experimental work. Interestingly, at smaller volumes, close to our previous EMTO or PAW equilibrium volumes, the $1Q$ magnetic configuration is lower in energy by a small amount. However, the frozen-core approximation corrects the lattice constant and therefore also the magnetic properties.

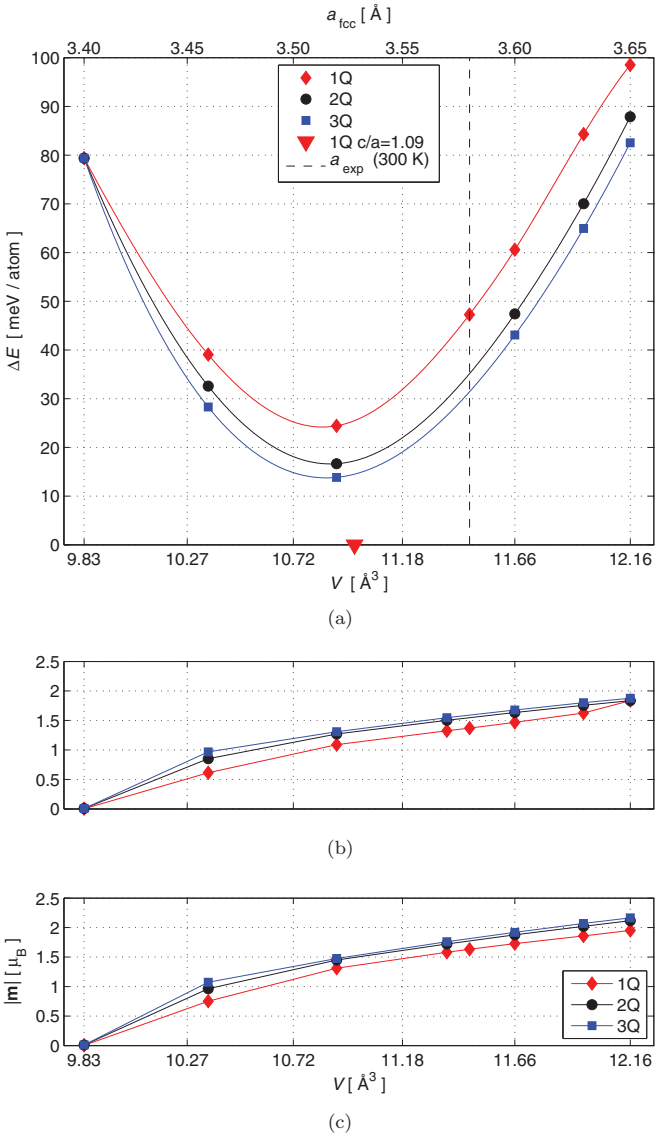

FIG. 12. (Color online) (a) Total energy and magnetic moments for (b) Fe and (c) Mn atoms in $Fe_{0.9}Mn_{0.1}$, calculated with the EMTO-CPA method, using the LSDA functional to compute the self-consistent charge density and magnetic moments, and then evaluating total energy using this charge density in the GGA functional. In (a) the total energy is shown for the cubic fcc structure assuming $1Q$ (red diamonds), $2Q$ (black circles), and $3Q$ (blue squares) magnetic structure, as a function of unit cell volume (lower horizontal scale) and the lattice constant (upper horizontal scale). The red triangle shows the total energy for the tetragonally distorted fct structure assuming $1Q$ ordering at the ground state volume. The experimental unit cell volume corresponding to 300 K is shown as a vertical dashed line.

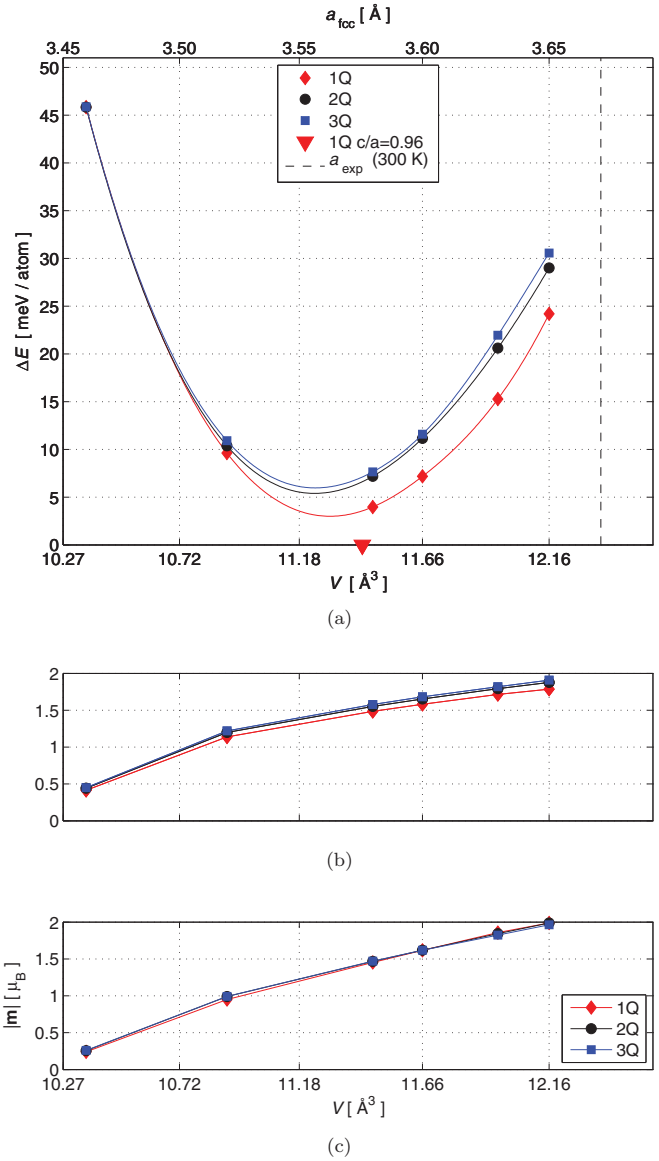

FIG. 13. (Color online) (a) Total energy and magnetic moments for (b) Fe and (c) Mn atoms in $Fe_{0.2}Mn_{0.8}$, calculated with the EMTO-CPA method, using the LSDA functional to compute the self-consistent charge density and magnetic moments, and then evaluating total energy using this charge density in the GGA functional. In (a) the total energy is shown for the cubic fcc structure assuming $1Q$ (red diamonds), $2Q$ (black circles), and $3Q$ (blue squares) magnetic structure, as a function of unit cell volume (lower horizontal scale) and the lattice constant (upper horizontal scale). The red triangle shows the total energy for the tetragonally distorted fct structure assuming $1Q$ ordering at the ground state volume. The experimental unit cell volume corresponding to 300 K is shown as a vertical dashed line.

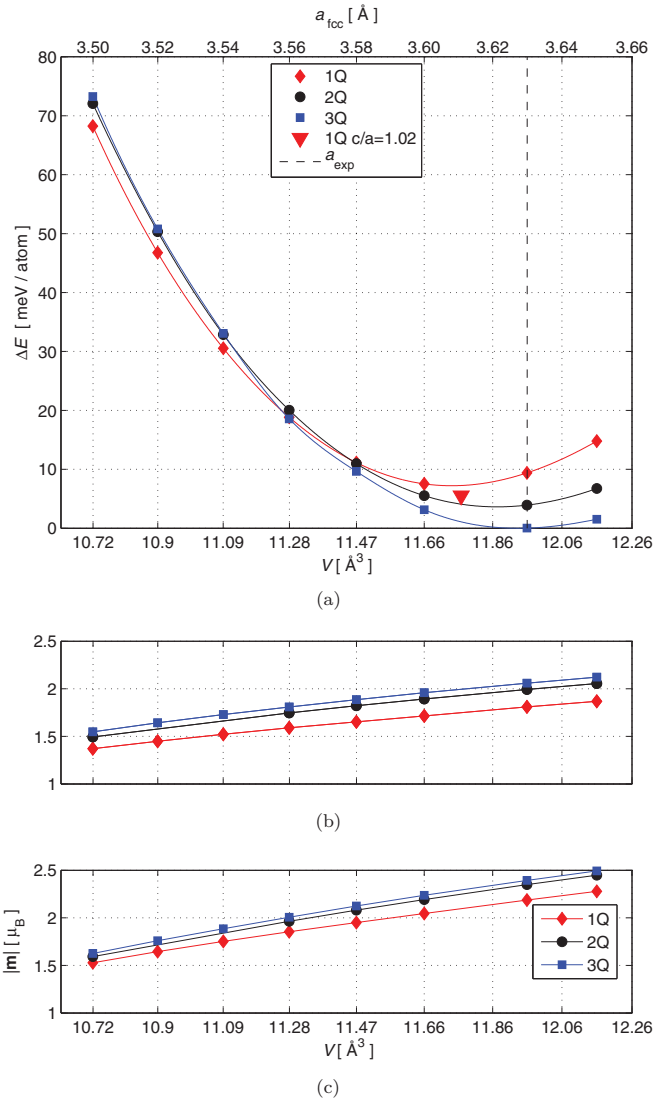

FIG. 14. (Color online) (a) Total energy and magnetic moments for (b) Fe (b) and (c) Mn atoms in $Fe_{0.5}Mn_{0.5}$, calculated with the EMTO-CPA method within the frozen-core approximation, using the PBE-GGA exchange-correlation functional. In (a) the total energy is shown for cubic fcc structure assuming $1Q$ (red diamonds), $2Q$ (black circles), and $3Q$ (blue squares) magnetic structure, as a function of unit cell volume (lower horizontal scale) and the lattice constant (upper horizontal scale). The red triangle shows the total energy for the tetragonally distorted fct structure assuming $1Q$ ordering at the ground state volume. The experimental unit cell volume corresponding to 0 K is shown as a vertical dashed line.

Relaxing the c/a ratio for the $1Q$ magnetic state we again find a slight tetragonal distortion, and the ground state value $(c/a)_0 = 1.02$, but as indicated in Fig. 14(a), this state is not lower in energy than the $3Q$ state on the cubic fcc lattice. It may also be pointed out that the unit cell volume obtained with this approximation, 11.8 Å^3, is also in rather good agreement with the experimental volume of 11.7 Å^3.

For fcc-$Fe_{0.9}Mn_{0.1}$, we obtain the lattice parameter 3.58 Å for the cubic fcc structure, as shown in Fig. 15(a), corresponding to the volume 11.5 Å^3. This is in good agreement with the experimental value, and also represents a significant improvement over the results reported in Sec. III C. However, the obtained ground state magnetic configuration is $3Q$ also with this approximation, which does not agree with the results reported in Ref. 10. Including tetragonal distortions in the $1Q$ magnetic state, the equilibrium volume increases slightly to

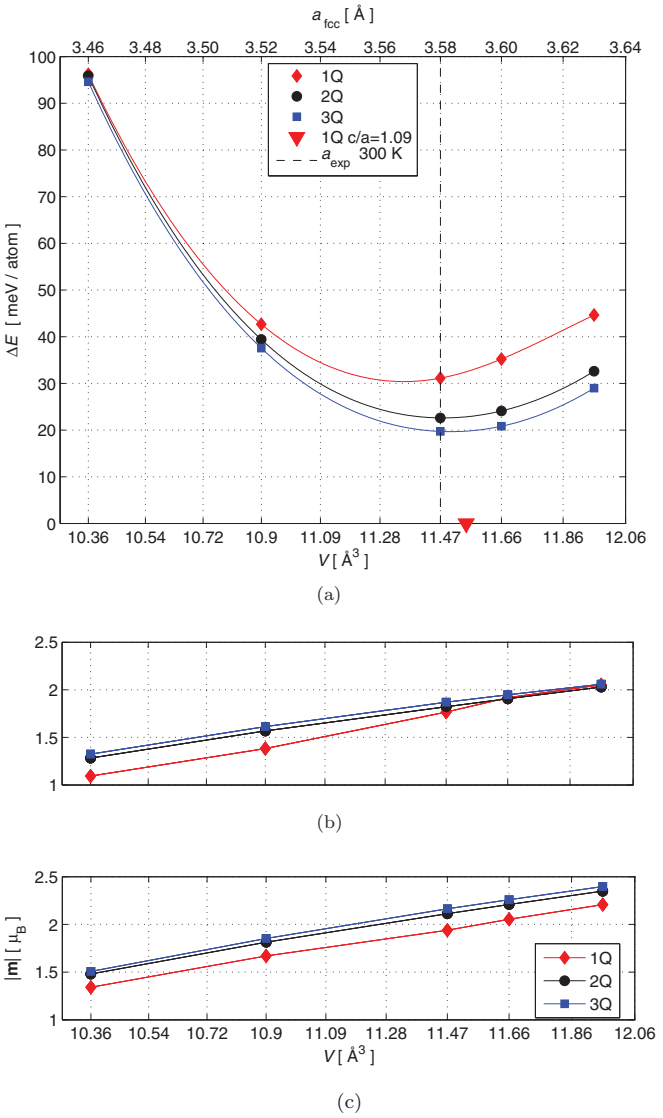

FIG. 15. (Color online) (a) Total energy and magnetic moments for (b) Fe (b) and (c) Mn atoms in $Fe_{0.9}Mn_{0.1}$, calculated with the EMTO-CPA method within the frozen-core approximation, using the PBE-GGA exchange-correlation functional. In (a) the total energy is shown for cubic fcc structure assuming $1Q$ (red diamonds), $2Q$ (black circles), and $3Q$ (blue squares) magnetic structure, as a function of unit cell volume (lower horizontal scale) and the lattice constant (upper horizontal scale). The red triangle shows the total energy for the tetragonally distorted fct structure assuming $1Q$ ordering at the ground state volume. The experimental unit cell volume corresponding to 300 K is shown as a vertical dashed line.

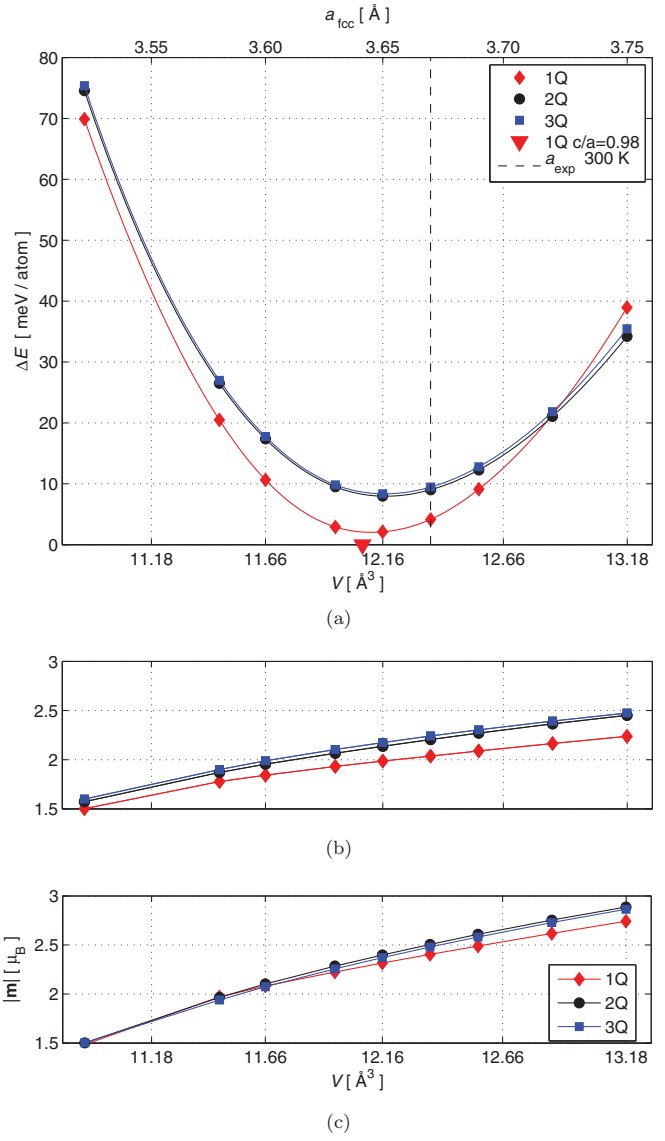

FIG. 16. (Color online) (a) Total energy and magnetic moments for (b) Fe (b) and (c) Mn atoms in $Fe_{0.2}Mn_{0.8}$, calculated with the EMTO-CPA method within the frozen-core approximation, using the PBE-GGA exchange-correlation functional. In (a) the total energy is shown for cubic fcc structure assuming $1Q$ (red diamonds), $2Q$ (black circles), and $3Q$ (blue squares) magnetic structure, as a function of unit cell volume (lower horizontal scale) and the lattice constant (upper horizontal scale). The red triangle shows the total energy for the tetragonally distorted fct structure assuming $1Q$ ordering at the ground state volume. The experimental unit cell volume corresponding to 300 K is shown as a vertical dashed line.

11.6 Å^3 with $(c/a)_0 = 1.09$, and this state is clearly lower in energy than $3Q$-fcc, as seen in Fig. 15(a).

Using the frozen-core approximation for fcc-$Fe_{0.2}Mn_{0.8}$ brings the lattice parameter to 3.65 Å for the $1Q$ magnetic state, as seen in Fig. 16(a), which is also in good agreement with experiment.[10] Allowing tetragonal relaxations, we find $(c/a)_0 = 0.98$, close to what was obtained in Fig. 10 without the frozen-core approximation, and the unit cell volume of 12.1 Å^3. This puts the EMTO frozen-core results in good agreement with the work of Endoh and Ishikawa,[10] who reported the unit cell volume of 12.3 Å^3.

In summary, we find that although the shape of the unit cell is slightly different to what was obtained in Secs. III B and III C, the frozen-core approximation in combination with the EMTO basis set corrects the alloy equilibrium volume and consequently the magnetic ground state configurations. For all the compositions considered in this work, the magnitude and volume dependence of the magnetic moments obtained within the frozen-core approximation are very similar to what was found with full EMTO calculations in Secs. III B and III C. The most probable reason for this is a somewhat

better cancellation of the errors obtained with this set of approximations. However, the cancellation is systematic, and is observed at all alloy compositions. But because of the increase of the unit cell volume, magnetic moments are clearly overestimated at equilibrium, as compared to experiment and LSDA calculations (Sec. III A) at the experimental volume. It should therefore be emphasized that, in contrast to the method proposed in Sec. III D 1, the approximation suggested in this section constitutes a pure computational simplification, which corrects the equilibrium volumes.

As the magnitudes of the ground state magnetic moments are overestimated within this scheme, we will now demonstrate how the frozen-core approximation in combination with the procedure outlined in the previous section may be combined in order to give accurate results for both magnetic and structural properties.

3. Proposed computational scheme for accurate theoretical simulations of Fe-Mn alloys

Having established the better description of equilibrium volumes within the frozen-core approximation (Sec. III D 2) and the better description of magnetic properties provided by the combined LSDA and GGA scheme (Sec. III D 1), we will now show that the two approximation sets can be used in a single scheme that accurately describes FeMn alloys in the complete composition interval. This scheme has previously been successfully used for calculations of elastic constants and thermodynamic properties in paramagnetic and AFM Fe-Mn alloys,[71–75] and will now be given its formal justification.

In Fig. 17(a) we show the total energy as a function of lattice constant for the $Fe_{0.5}Mn_{0.5}$ alloy. We again see that the experimental lattice constant is reproduced quite well, and the ground state magnetic configuration is again $3Q$, as obtained with LSDA and GGA when the lattice constant is fixed to this value in Secs. III B 1 and III C. The results concerning volume obtained with the present method thus agree with the scheme used in Sec. III D 2, where the GGA functional was used to obtain both charge density and total energy [Fig. 14(a)] in combination with the frozen-core approximation. Magnetic moments are, however, lower since the LSDA is used for charge density, and thus magnetization. This improves the agreement with experiment.

For the $Fe_{0.9}Mn_{0.1}$ alloy, the results for the total energy are presented in Fig. 18. In the case of cubic fcc structure, the system adopts the noncollinear $3Q$ order and the room-temperature lattice constant is well reproduced. Allowing tetragonal distortions leads to the overall ground state in the $1Q$ configuration, with the unit cell volume 11.6 Å^3, which is close to the experimental volume of the fcc phase.

In the Mn-rich alloy $Fe_{0.2}Mn_{0.8}$, we recover $1Q$ as the ground state magnetic configuration in the cubic fcc phase, as shown in Fig. 19. The lattice constant is close to the experimental value. Allowing tetragonal distortions correctly contracts the lattice along the direction of the spin density wave, while essentially preserving the unit cell volume. For both of the off-stoichiometric compositions, we again observe how the magnetic moments are lower compared with what is shown in Figs. 15 and 16.

For pure fct-Mn we obtain the unit cell volume of 12.2 Å^3 in the $1Q$ magnetic configuration with $(c/a)_0 = 0.94$, which is

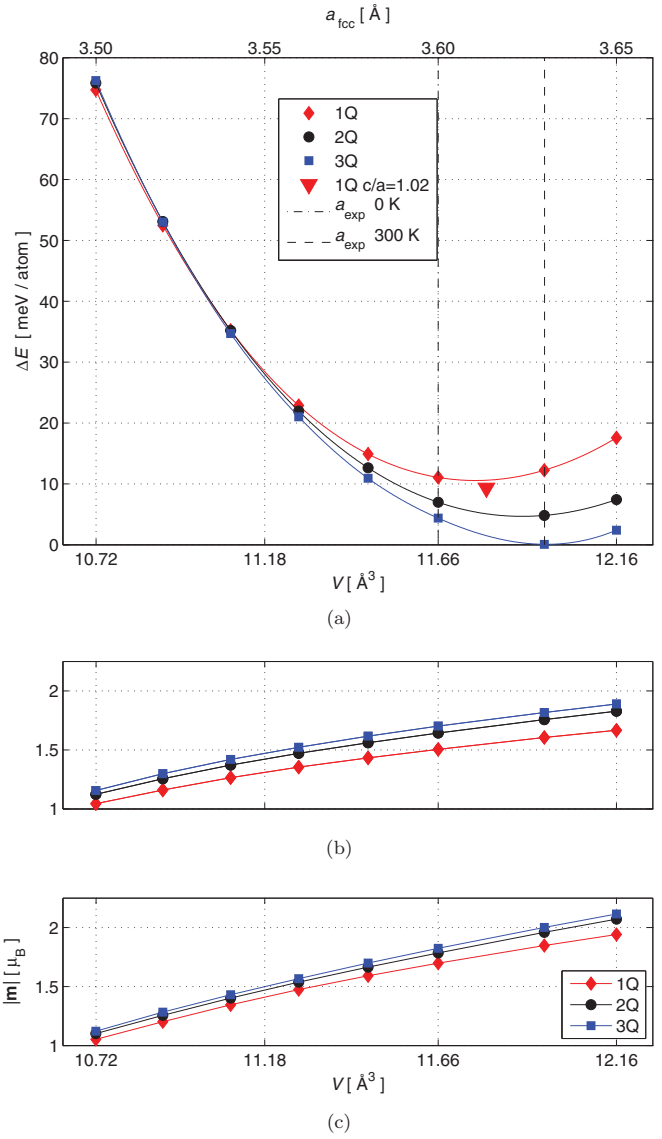

FIG. 17. (Color online) (a) Total energy and magnetic moments for (b) Fe (b) and (c) Mn atoms in $Fe_{0.5}Mn_{0.5}$, calculated with the EMTO-CPA method within the frozen-core approximation, using the LSDA functional to compute the self-consistent charge density and magnetic moments, and then evaluating total energy using this charge density in the GGA functional. In (a) the total energy is shown for cubic fcc structure assuming $1Q$ (red diamonds), $2Q$ (black circles), and $3Q$ (blue squares) magnetic structure, as a function of unit cell volume (lower horizontal scale) and the lattice constant (upper horizontal scale). The red triangle shows the total energy for the tetragonally distorted fct structure assuming $1Q$ ordering at the ground state volume. The experimental unit cell volume corresponding to 0 and 300 K are shown as dash-dotted and dashed vertical lines, respectively.

a significant improvement compared with earlier results. The magnetic moment is 2.3 μ_B, which is within the experimental interval, as reported in Ref. 23. In cubic $1Q$-ordered fcc-Fe we find the unit cell volume 11.3 Å^3, and allowing tetragonal distortions we find the volume 11.6 Å^3 with $(c/a)_0 = 1.1$, which is close to the value of 11.4 Å^3 that has been reported in low-temperature measurements.[62,76] Thus, the proposed scheme can be used in the entire composition interval of FeMn alloys.

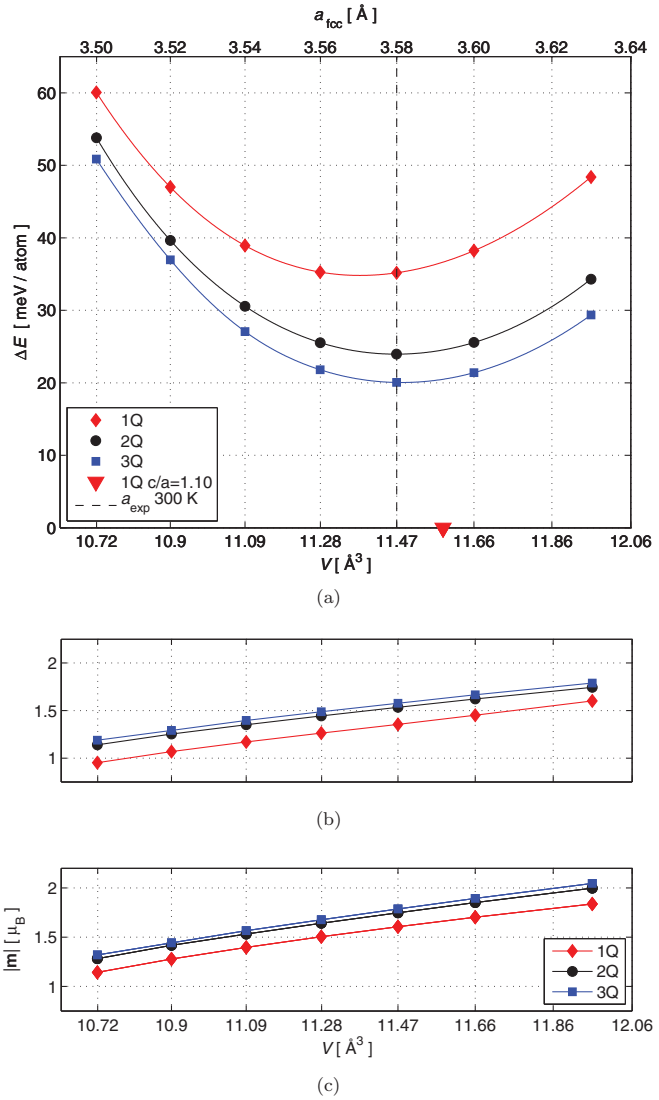

FIG. 18. (Color online) (a) Total energy and magnetic moments for (b) Fe (b) and (c) Mn atoms in $Fe_{0.9}Mn_{0.1}$, calculated with the EMTO-CPA method within the frozen-core approximation, using the LSDA functional to compute the self-consistent charge density and magnetic moments, and then evaluating total energy using this charge density in the GGA functional. In (a) the total energy is shown for cubic fcc structure assuming $1Q$ (red diamonds), $2Q$ (black circles), and $3Q$ (blue squares) magnetic structure, as a function of unit cell volume (lower horizontal scale) and the lattice constant (upper horizontal scale). The red triangle shows the total energy for the tetragonally distorted fct structure assuming $1Q$ ordering at the ground state volume. The experimental unit cell volume corresponding to 300 K is shown as a vertical dashed line.

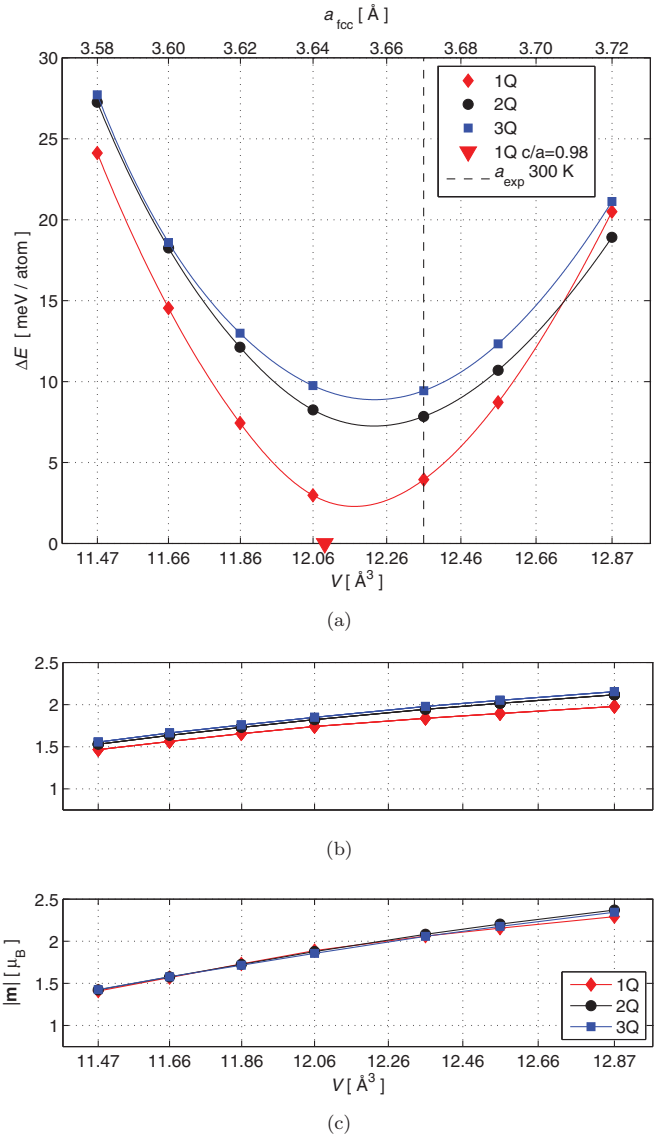

FIG. 19. (Color online) (a) Total energy and magnetic moments for (b) Fe (b) and (c) Mn atoms in $Fe_{0.2}Mn_{0.8}$, calculated with the EMTO-CPA method within the frozen-core approximation, using the LSDA functional to compute the self-consistent charge density and magnetic moments, and then evaluating total energy using this charge density in the GGA functional. In (a) the total energy is shown for cubic fcc structure assuming $1Q$ (red diamonds), $2Q$ (black circles), and $3Q$ (blue squares) magnetic structure, as a function of unit cell volume (lower horizontal scale) and the lattice constant (upper horizontal scale). The red triangle shows the total energy for the tetragonally distorted fct structure assuming $1Q$ ordering at the ground state volume. The experimental unit cell volume corresponding to 300 K is shown as a vertical dashed line.

In summary, we see that the results concerning the ground state volumes are very similar to those obtained in Sec. III D 2 using the frozen-core approximation but with the GGA functional for both charge density and total energy. However, an important difference is found when comparing Figs. 17–19 (b),(c), showing the magnetic moments, which are in closer agreement with experimental data than what was found using the GGA in Figs. 14–16 (b),(c). This is not surprising since we have previously seen that GGA overestimates magnetic moments. Especially since use of the frozen-core approximation in EMTO calculations increases equilibrium volumes, improving their agreement with experimental data, it is essential to use the LSDA functional for charge density, which gives a better description of magnetic properties at fixed volume.

IV. SUMMARY AND CONCLUSION

We have investigated the magnetic ground state of γ FeMn alloys taking into account simultaneous global, as well as local, relaxations of the crystal lattice and magnetic moments. Using complementary state-of-the-art *ab initio* electronic structure codes, we find the magnetic ground state to depend strongly on the lattice constant used in the calculation. For $Fe_{0.5}Mn_{0.5}$ at experimental volumes, we obtain the $3Q$ magnetic state as the ground state, regardless of the approximation for the exchange-correlation functional, or if local lattice relaxations and local magnetic reorientations are included.

Similar to previous studies of Fe and γ-Mn (Refs. 37 and 77), we find that the LSDA functional severely underestimates the equilibrium volumes. However, use of the GGA functional does not remedy the problem as it does for bcc-Fe, and consequently, the obtained magnetic properties at the theoretical volumes differ from those found at the experimental lattice spacing. In fact, the results for magnetic properties depend not only on the type of exchange-correlation functional (LSDA or GGA), but also on the particular choice of GGA parametrization. Using the PBE parametrization we find the $1Q$ state to be the ground state, while the PW91 parametrization favors $3Q_R$ magnetic configuration on the ideal fcc lattice and makes $1Q$ and $3Q_R$ states degenerate if local lattice relaxations are included. This sensitivity to the GGA parametrization has also been reported for fcc-Fe (Ref. 61). By varying the composition of the alloy, we find that the error in the lattice parameter increases with increasing Mn concentration. Since electron correlations in $1Q$ fcc-Mn have been shown to be inaccurately described by the local or semi-local DFT exchange-correlation functionals, causing the lattice constant to be drastically underestimated,[37,77] one may conclude that correlation effects, although less dramatic than in f-electron systems, are still very important in Fe-based $3d$ systems and that the FeMn alloy may not always be accurately described using standard *ab initio* computational techniques.

Therefore, due to the need for efficient computational tools for modeling of FeMn alloys and steels, we have suggested a practical computational scheme which may be successfully used for the FeMn system without the tremendous computational cost of considering strong many-body effects. The scheme is based on a combination of physical arguments and methodological simplifications, which gives very good cancellation of errors in the entire composition interval. In the proposed scheme, the LSDA functional is used to self-consistently calculate the nonspherical ground state charge density, which is then used in the GGA functional for evaluation of total energy. This approach reproduces the energetics given by the GGA, and has the LSDA accuracy for magnetic properties. In addition, we employ the frozen-core approximation in combination with the EMTO basis set, which corrects the lattice parameters in the entire composition range, and recovers the magnetic ground state obtained using LSDA or GGA at the experimental lattice constants. We therefore suggest that this scheme can be used for practical purposes in modeling of FeMn alloys without any further adjustable parameters.

ACKNOWLEDGMENTS

Calculations were performed at the facilities of the National Supercomputing Centre in Sweden (NSC) and High Performance Computing Center North (HPC2N). This project was funded by the Göran Gustafsson Foundation for Research in Natural Sciences and Medicine and by the Swedish e-Science Research Centre (SeRC).

*marekh@ifm.liu.se

[1] U. Brüx, G. Frommeyer, O. Grässel, L. W. Meyer, and A. Weise, Steel Research **73**, 294 (2002).
[2] G. Frommeyer, U. Brüx, and P. Neumann, ISIJ International **43**, 438 (2003).
[3] J. Kools, IEEE Trans. Magn. **32**, 3165 (1996).
[4] B. Dieny, V. S. Speriosu, S. S. P. Parkin, B. A. Gurney, D. R. Wilhoit, and D. Mauri, Phys. Rev. B **43**, 1297 (1991).
[5] J. Nogués and I. K. Schuller, J. Magn. Mag. Mat. **192**, 203 (1991).
[6] C. Mitsumata, A. Sakuma, and K. Fukamichi, IEEE Trans. Magn. **39**, 2738 (2003).
[7] C. Mitsumata, A. Sakuma, and K. Fukamichi, J. Phys. Soc. Jpn. **76**, 024704 (2007).
[8] J. S. Kouvel and J. S. Kasper, J. Phys. Chem. Solids **24**, 529 (1963).
[9] H. Umebayashi and Y. Ishikawa, J. Phys. Soc. Jpn. **21**, 1281 (1966).
[10] Y. Endoh and Y. Ishikawa, J. Phys. Soc. Jpn. **30**, 1614 (1971).
[11] K. Tajima, Y. Ishikawa, Y. Endoh, and Y. Noda, J. Phys. Soc. Jpn. **41**, 1195 (1976).
[12] P. Bisanti *et al.*, J. Phys. F **17**, 1425 (1987).
[13] S. J. Kennedy and T. J. Hicks, J. Phys. F **17**, 1599 (1987).
[14] S. Kawarazaki, Y. Sasaki, K. Yasuda, T. Mizusaki, and A. Hirai, J. Phys. Condens. Matter **2**, 5747 (1990).
[15] J. Kubler, K. H. Hock, J. Sticht, and A. R. Williams, J. Phys F **18**, 469 (1988).
[16] S. Fujii, S. Ishida, and S. Asano, J. Phys. Soc. Jpn. **60**, 4300 (1991).
[17] A. Sakuma, J. Phys. Soc. Jpn. **69**, 3072 (2000).
[18] K. Nakamura, T. Ito, A. J. Freeman, L. Zhong, and J. Fernandez-de-Castro, Phys. Rev. B **67**, 014405 (2003).
[19] D. Spišák and J. Hafner, Phys. Rev. B **61**, 11569 (2000).
[20] D. D. Johnson, F. J. Pinski, and G. M. Stocks, J. Appl. Phys. **63**, 3490 (1988).
[21] T. C. Schulthess, W. H. Butler, G. M. Stocks, S. Maat, and G. J. Mankey, J. Appl. Phys. **85**, 4842 (1999).
[22] G. M. Stocks, W. A. Shelton, T. C. Schulthess, B. Újfalussy, W. H. Butler, and A. Canning, J. Appl. Phys. **91**, 7355 (2002).
[23] J. Kübler, *Theory of Itinerant Electron Magnetism* (Oxford Science Publications, Oxford, 2000).
[24] *Binary Alloy Phase Diagrams*, edited by T. Massalki, J. L. Murrat, L. H. Bennet, and H. Baker (American Society for Metals Russell Township, OH, 1986).
[25] C. S. Smith, Phys. Rev. **57**, 337 (1940).

[26]S. C. Abrahams, L. Guttman, and J. S. Kasper, Phys. Rev. **127**, 2052 (1962).
[27]E. I. Kondorskii and V. L. Sedov, Sov. Phys. JETP **8**, 1104 (1959).
[28]W. A. A. Macedo and W. Keune, Phys. Rev. Lett. **61**, 475 (1988).
[29]U. Gonser, C. J. Meechan, A. H. Muir, and H. Wiedersich, J. Appl. Phys. **34**, 2373 (1963).
[30]G. J. Johanson, M. B. McGirr, and D. A. Wheeler, Phys. Rev. B **1**, 3208 (1970).
[31]Y. Tsunoda, H. Nogami, and M. Takasaka, Phys. Rev. B **76**, 054419 (2007).
[32]E. Sjöstedt and L. Nordström, Phys. Rev. B **66**, 014447 (2002).
[33]K. Knöpfle, L. M. Sandratskii, and J. Kübler, Phys. Rev. B **62**, 5564 (2000).
[34]M. Marsman and J. Hafner, Phys. Rev. B **66**, 224409 (2002).
[35]Y. Tsunoda, J. Phys. F **18**, L251 (1988).
[36]Y. Tsunoda, J. Phys. Condens. Matter **51**, 10427 (1989).
[37]I. Di Marco, J. Minár, S. Chadov, M. I. Katsnelson, H. Ebert, and A. I. Lichtenstein, Phys. Rev. B **79**, 115111 (2009).
[38]S. Biermann *et al*., JETP Lett. **80**, 612 (2004).
[39]P. E. Blöchl, Phys. Rev. B **50**, 17953 (1994).
[40]G. Kresse and D. Joubert, Phys. Rev. B **59**, 1758 (1999).
[41]G. Kresse and J. Hafner, Phys. Rev. B **47**, 558 (1993).
[42]G. Kresse and J. Furthmüller, Comput. Mater. Sci. **6**, 15 (1996).
[43]G. Kresse and J. Furthmüller, Phys. Rev. B **54**, 11169 (1996).
[44]L. Vitos, Phys. Rev. B **64**, 014107 (2001).
[45]L. Vitos, *Computational Quantum Mechanics for Materials Engineers: the EMTO Method and Applications* (Springer-Verlag, London, 2007).
[46]L. Vitos, J. Kollár, and H. L. Skriver, Phys. Rev. B **55**, 13521 (1997).
[47]A. Zunger, S. H. Wei, L. G. Ferreira, and J. E. Bernard, Phys. Rev. Lett. **65**, 353 (1990).
[48]I. A. Abrikosov, S. I. Simak, B. Johansson, A. V. Ruban, and H. L. Skriver, Phys. Rev. B **56**, 9319 (1997).
[49]P. E. Blöchl, O. Jepsen, and O. K. Andersen, Phys. Rev. B **49**, 16223 (1994).
[50]M. Methfessel and A. T. Paxton, Phys. Rev. B **40**, 3616 (1989).
[51]H. J. Monkhorst and J. D. Pack, Phys. Rev. B **13**, 5188 (1976).
[52]J. P. Perdew and Y. Wang, Phys. Rev. B **45**, 13244 (1992).
[53]J. P. Perdew, K. Burke, and M. Ernzerhof, Phys. Rev. Lett. **77**, 3865 (1996).
[54]S. H. Vosko, L. Wilk, and M. Nusair, Can. J. Phys. **58**, 1200 (1980).
[55]D. M. Ceperley and B. J. Alder, Phys. Rev. Lett. **45**, 566 (1980).
[56]L. M. Sandratskii, J. Phys. Condens. Matter **3**, 8565 (1991).
[57]L. Vitos, I. A. Abrikosov, and B. Johansson, Phys. Rev. Lett. **87**, 156401 (2001).
[58]L. Vitos, I. A. Abrikosov, and B. Johansson, in *Complex Inorganic Solids*, edited by P. E. A. Turchi, A. Gonis, K. Rajan, and A. Meike, (Springer, New York, 2005).
[59]A. V. Ruban and I. A. Abrikosov, Rep. Prog. Phys. **71**, 046501 (2008).
[60]P. Marinelli, A. Baruj, A. F. Guillermet, and M. Sade, Z. Metallkd. **91**, 957 (2000).
[61]I. A. Abrikosov, A. E. Kissavos, F. Liot, B. Alling, S. I. Simak, O. Peil, and A. V. Ruban, Phys. Rev. B **76**, 014434 (2007).
[62]P. Ehrhart, B. Schönfeld, H. Ettwig, and W. Pepperhoff, J. Magn. Magn. Mater. **22**, 79 (1980).
[63]S. S. Peng and H. J. F. Jansen, J. App. Phys. **69**, 6132 (1991).
[64]S. L. Qiu and P. M. Marcus, Phys. Rev. B **60**, 14533 (1999).
[65]D. Spišák and J. Hafner, Phys. Rev. B **61**, 16129 (2000).
[66]T. Oguchi and A. Freeman, J. Magn. Magn. Mater. **46**, L1 (1984).
[67]M. Uhl and J. Kübler, J. Phys. Condens. Matter **9**, 7885 (1997).
[68]S. L. Qiu, P. M. Marcus, and H. Ma, Phys. Rev. B **62**, 3292 (2000).
[69]J. Hafner and D. Spišák, Phys. Rev. B **72**, 144420 (2005).
[70]A. V. Ruban, S. Khmelevskyi, P. Mohn, and B. Johansson, Phys. Rev. B **76**, 014420 (2007).
[71]D. Music, T. Takahashi, L. Vitos, C. Asker, I. A. Abrikosov, and J. M. Schneider, Appl. Phys. Lett. **91**, (2007).
[72]T. Gebhardt, D. Music, B. Hallstedt, M. Ekholm, I. A. Abrikosov, L. Vitos, and J. M. Schneider, J. Phys. Condens. Matter **22**, 295402 (2010).
[73]T. Gebhardt, D. Music, M. Ekholm, I. A. Abrikosov, J. von Appen, R. Dronskowski, D. Wagner, J. Mayer, and J. M. Schneider, Acta Mater. **59**, 1493 (2011).
[74]T. Gebhardt, D. Music, D. Kossmann, M. Ekholm, I. A. Abrikosov, L. Vitos, and J. M. Schneider, Acta Mater. **59**, 3145 (2011).
[75]T. Gebhardt, D. Music, M. Ekholm, I. A. Abrikosov, L. Vitos, A. Dick, T. Hickel, J. Neugebauer, and J. M. Schneider, J. Phys: Condens. Matter **23**, 246003 (2011).
[76]Y. Tsunoda, N. Kunitomi, and R. M. Nicklow, J. Phys. F **17**, 2447 (1987).
[77]M. Eder, J. Hafner, and E. G. Moroni, Phys. Rev. B **61**, 11492 (2000).